Available online at www.sciencedirect.com
SCIENCE DIRECT®
Journal of Molecular Catalysis A: Chemical 231 (2005) 145–151
JOURNAL OF MOLECULAR CATALYSIS A: CHEMICAL
www.elsevier.com/locate/molcata

Catalytic performance of zirconium-modified Co/Al_2O_3 for Fischer–Tropsch synthesis

Haifeng Xiong, Yuhua Zhang, Kongyong Liew, Jinlin Li*

Hubei Key Laboratory for Catalysis and Material Science, College of Chemistry and Material Science, South-Central University for Nationalities, Wuhan 430074, China

Received 11 October 2004; received in revised form 15 December 2004; accepted 18 December 2004

Abstract

A series of zirconium-modified Co/Al_2O_3 catalysts were prepared with a two-step impregnation method using the incipient wetness technique. XRD, XPS, TPR, H_2-TPD and oxygen titration were used for the characterization of the catalysts. The catalytic performance was performed in a fixed bed reactor for Fischer–Tropsch synthesis (FTS). The $CoAl_2O_4$ spinel phase was detected on the prepared catalysts and its content on the catalysts decreased with the increase of zirconium loading, indicating that Zr-added could inhibit $CoAl_2O_4$ formation. The addition of zirconium to the Co catalyst caused the increase of cobalt cluster size. Zr addition has been shown to improve the activity and C_{5+} selectivity of Co/Al_2O_3 catalyst for Fischer–Tropsch synthesis. This could be explained by the increase of active metal cobalt site and reducibility. The increase of zirconium loading on $Co/Zr/Al_2O_3$ catalyst resulted in the increase of olefin/paraffin ratio in the products.

Keywords: Fischer–Tropsch synthesis; Cobalt/alumina; Zirconium; Reducibility; Olefin/paraffin

1. Introduction

Fischer–Tropsch synthesis (FTS) has been a promising process for the conversion of coal and natural gas to liquid fuel since it is commercialization. Metallic Co, Ni, Ru, etc. are usually used as FTS catalysts. The cobalt catalyst is preferred due to its high selectivity for heavy hydrocarbons, low activity for the water–gas shift (WGS) reaction and lower price than ruthenium [1,2]. For cobalt FTS catalyst, the effect of supports such as Al_2O_3 [3], TiO_2 [4], SiO_2 [5], etc. have been investigated. Al_2O_3 is usually adopted as the support to prepare cobalt catalysts due to the excellent texture even though the catalyst exhibited limited reducibility because of the strong interaction between the cobalt and the alumina support. The reducibility of cobalt-based catalyst can be improved to a certain extent by promotion with metal or metal oxide such as Pt [6], Re [7], ZrO_2 [8], etc.

A number of investigations have been focused on zirconium as a promoter for the supported cobalt catalysts. However, it is not clear how it worked and different researcher has different opinions. Andreas et al. [9] reported that a weaker cobalt–zirconium interaction was observed and the addition of zirconium led to the increase of reducibility. Moradi et al. [8] claimed that the interaction of cobalt–silica is replaced by the Co–Zr interaction which favors the reduction of the catalysts at lower temperature. However, according to the literatures [10,11], Co/ZrO_2 catalyst calcined at 673 K did not form cobalt zirconate and Co compounds were completely reduced to metallic cobalt.

Zr-promoted Co catalysts were found to have higher activity and C_{5+} selectivity for FTS than nonpromoted catalysts [8]. Ali et al. [12] reported that zirconium promotion possibly created an active interface with Co that increased activity by facilitating CO dissociation. Rohr et al. [13] studied the modification by ZrO_2 of Co/Al_2O_3 catalyst and concluded that the addition of zirconium increased the activity and selectivity to heavy hydrocarbon, while reducibility and dispersion have

* Corresponding author. Tel.: +86 27 67843016; fax: +86 27 67842752.
E-mail address: lij@scuec.edu.cn (J. Li).

1381-1169/$ – see front matter © 2005 Elsevier B.V. All rights reserved.
doi:10.1016/j.molcata.2004.12.033

not been improved. They ascribed it to the coverage effect rather than the intrinsic activity of the active sites. It is therefore important to obtain a full understanding of the influence of Zr on the activity and selectivity of FTS catalysts.

The present work attempts to explain the role of zirconium as a promoter for Fischer–Tropsch synthesis over alumina supported cobalt catalyst. The prepared catalysts were characterized by XRD, XPS, TPR, TPD, O_2 titration and their catalytic performances were tested in a fixed bed reactor.

2. Experimental

2.1. Catalyst preparation

The catalysts were prepared by incipient wetness impregnation of γ-Al_2O_3 support (Institute of Shandong Alumina, China, BET surface area 230 $m^2\,g^{-1}$, average particle size 0.4–0.6 mm, pore volume 0.401 $cm^3\,g^{-1}$) with aqueous cobalt nitrate ($Co(NO_3)_2{\cdot}6H_2O$) and zirconium nitrate ($Zr(NO_3)_4{\cdot}5H_2O$) solutions. The Al_2O_3 support was first calcined at 873 K in flowing air for 6 h before impregnation. For Co/Al_2O_3 catalyst, cobalt nitrate was dissolved in deionized water and directly impregnated into the support using incipient wetness. For the promoted catalysts, zirconium was added to the Al_2O_3 support prior to the addition of Co. The zirconium nitrate was dissolved in an appropriate volume of deionized water and impregnated onto the Al_2O_3 support. Subsequently, the precursor was aged for 12 h in air at room temperature, followed by drying at 393 K for 12 h. To prepare catalysts with higher zirconium contents (>5 wt.%), the procedure involving impregnation and drying was repeated several times. The precursors were then calcined at 823 K for 6 h. All the catalysts promoted with various percentages of zirconium (0.5, 1, 5, 9, 15 wt.%) contained 15 wt.% Co. To obtain 15 wt.% cobalt loading for all samples, a two-step incipient wetness impregnation method was used with drying at 393 K following each impregnation. Finally, all catalysts were dried at 393 K for 12 h and calcined in air at 623 K for 6 h. In this study, the reduced catalysts containing *x*% Co and *y*% Zr will be denoted as *x*Co/*y*Zr/Al_2O_3.

2.2. Characterization

2.2.1. BET measurements

Pore size distribution, BET surface area and pore volume were measured by Micromeritics ASAP2405 using nitrogen adsorption at 77 K. Prior to the measurements, the sample was degassed for 4 h at 373 K in flowing helium (30 $cm^3\,min^{-1}$).

2.2.2. Temperature programmed reduction (TPR)

The reduction behavior and the interaction between active phase and support of each catalyst were examined by using temperature programmed reduction (TPR) technique. The TPR experiment was carried out with a Zeton Altamira AMI-200 unit. The catalyst (ca. 0.15 g) was placed in a quartz tubular reactor, fitted with a thermocouple for continuous temperature measurement. The reactor was heated with a furnace designed and built to stabilize the temperature gradient and minimize the temperature error. Prior to the hydrogen temperature programmed reduction measurement, the calcined catalysts were flushed with high purity argon at 423 K for 1 h, to drive away the water or impurities, and then, cooled down to 323 K. Then 10% H_2/Ar was switched on and the temperature was raised at a rate of 10 K min^{-1} from 323 to 1023 K (hold 30 min). The gas flow rate through the reactor was controlled by three Brooks mass flow controllers (MFCs) and was always 30 $cm^3\,min^{-1}$. The H_2 consumption (TCD signal) was recorded automatically by a PC.

2.2.3. Hydrogen temperature programmed desorption (H_2-TPD) and O_2 titration

Hydrogen temperature programmed desorption was also carried out in a U-tube quartz reactor with the Zeton Altamira AMI-200 unit. The sample weight was about 0.200 g. The catalyst was reduced at 723 K for 12 h using a flow of high purity hydrogen and then cooled to 373 K under hydrogen stream. The sample was held at 373 K for 1 h under flowing argon to remove weakly bound physisorbed species prior to increasing the temperature slowly to 723 K. At that temperature, the catalyst was held under flowing argon to desorb the remaining chemisorbed hydrogen and the TCD began to record the signal till the signal returned to the baseline. The TPD spectrum was integrated and the amount of desorbed hydrogen were determined by comparing to the mean areas of calibrated hydrogen pulses. Prior to the experiments, the sample loop was calibrated with pulses of nitrogen in helium flow, comparing with the signal produced from a gas tight syringe injection (100 μl) of nitrogen under helium flow.

O_2 titration was also performed with the Zeton Altamira AMI-200 unit. The extent of cobalt reduction was determined by O_2 titration of reduced samples at 723 K. After reduction under the conditions (as described above for H_2-TPD), the catalysts were kept in flowing Ar at 723 K and the sample was reoxidized by injecting pulses of high purity oxygen in argon. The extent of reduction was calculated by assuming metal Co was converted to Co_3O_4. All flow rates were set to 30 $cm^3\,min^{-1}$. The uncorrected dispersions (cluster size) are based on the assumption of complete reduction, and the corrected dispersions are reported by percentage reduction. The formula for the calculation has been shown in previous studies [14,16].

2.2.4. X-ray powder diffraction (XRD)

X-ray powder diffraction (XRD) spectra for the calcined catalysts were recorded with a Philips X'pert PRO using Cu Kα radiation and Ni filter. The scan range was 10–90° with 0.002° steps. Crystallite phases were detected by comparing the diffraction patterns with those in the standard powder XRD file compiled by the Joint Committee on Powder Diffraction Standards (JCPDSs) published by the Interna-

tional Center for Diffraction Data. Average Co_3O_4 crystallite size was calculated using the Scherrer equation [15] from the most intense Co_3O_4 peak ($2\theta = 36.8^\circ$).

$$d = \frac{k\lambda}{B\cos\theta}\frac{180^\circ}{\pi}$$

where d is the mean crystallite diameter, k (0.89) is the Scherrer constant, λ is the X-ray wave length (1.54056 Å), and B is the full width half maximum (FWHM) of Co_3O_4 diffraction peak.

2.2.5. X-ray photoelectron spectroscopy (XPS)

The surface composition of the catalysts were determined from X-ray photoelectron spectroscopy (XPS), performed by a Vacuum Generator ESCALAB-MKII spectrometer with a monochromatized Al Kα source (1486.6 eV) at the constant analyzer pass energy of 20.0 eV. The binding energy is estimated to be accurate within 0.2 eV. All binding energies (BEs) were corrected referencing to the C 1s (284.6 eV) peak of the contamination carbon as an internal standard. The Co 2p binding energy of the core level was determined by computer fitting of the measured spectra.

2.3. F–T activity and selectivity

Fischer–Tropsch synthesis was performed in a fixed bed reactor (i.d. 2 cm) at 10 bar. The catalyst (ca. 6.0 g) was mixed with ca. 36.0 g carborundum and reduced at atmosphere pressure in situ. The reactor temperature was increased from ambient to 373 K (hold 60 min) in 6 SL h^{-1} g^{-1} flow of H_2, then, increased to 723 K in 2 h and held at that temperature for 10 h. Subsequently, the reactor was cooled down to 453 K. After reduction, the syngas (H_2:CO = 2) was introduced to the reactor and the pressure was increased to 10 bar. The reactor temperature was raised to 483 K at 1 K min^{-1}, then, increased to 503 K in 4 h and the reaction was carried out at 503 K. The products were collected in a hot trap (403 K) and a cold trap (271 K) in sequence.

The effluent product gas was passed through an Agilent 3000GC for online analysis. The liquid product (collected at 271 K) analysis was performed with an Agilent 6890GC equipped with a FID detector. The solid wax (collected at 403 K) was dissolved in dimethylbenzene, and analyzed with an Agilent 4890GC. The carbon monoxide conversion (X_{CO}%) was measured at the steady state and X_{CO}%, hydrocarbon selectivity have been averaged over the period of constant operation. The ratio of olefin/paraffin was calculated from the respective chromatogram peak areas.

3. Results and discussion

3.1. BET surface area

The BET surface areas, pore volume, average pore diameter of the catalysts are summarized in Table 1. With increasing amount of zirconium impregnated, more of the pores of Al_2O_3 support were blocked. Thus, the average pore volume and the BET surface area decrease, while the pore diameter remains relatively unchanged.

Table 1
BET measurements

Sample	S_{BET} (m^2 g^{-1})	Pore volume (cm^3 g^{-1})	Pore diameter (nm)
$15Co/Al_2O_3$	144	0.38	10.5
$15Co/1Zr/Al_2O_3$	159	0.40	10.0
$15Co/5Zr/Al_2O_3$	133	0.35	10.4
$15Co/9Zr/Al_2O_3$	123	0.31	10.2

3.2. X-ray diffraction (XRD)

The XRD patterns of the catalysts are shown in Fig. 1. The diffraction peaks at 45.66° and 66.6° are due to the Al_2O_3 support, while other peaks are reasonably assigned to the spinel phases of Co_3O_4 and the different crystal phase of Co_3O_4–Al_2O_3 interaction species [16] including $CoAl_2O_4$. No Co–Zr interaction compound can be detected. From the XRD patterns of $Co/Zr/Al_2O_3$ catalysts and the ZrO_2/Al_2O_3 precursor (figure not shown here), the diffraction peak of ZrO_2 phase cannot be detected, indicating that the ZrO_2 is highly dispersed on the support [17]. As can be seen, the different catalysts have basically the same pattern of peak intensities as that of the cubic spinel phase of Co_3O_4 and $CoAl_2O_4$. It is difficult to establish the chemical and structural phases for those catalysts based only on the XRD characteristic because both Co_3O_4 and $CoAl_2O_4$ have cubic spinel structure with almost identical diffraction peak position. However, this can be resolved by the following XPS technique.

Table 2 shows the average size of the Co_3O_4 crystal of the different catalysts. It is clear that the Co_3O_4 size increases with the increase of zirconium on catalysts.

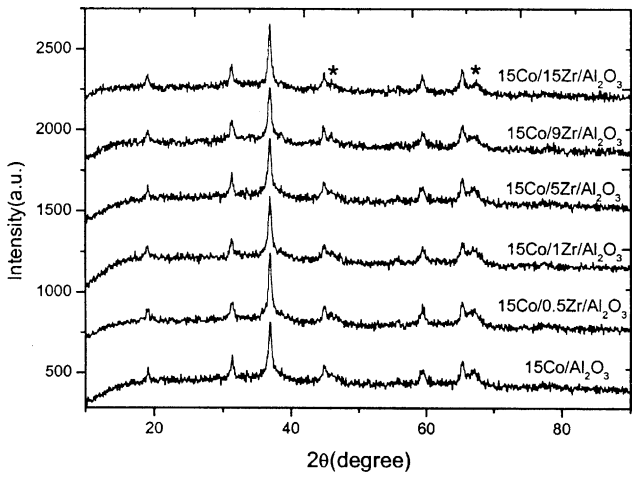

Fig. 1. Powder XRD patterns of catalysts with different Zr content (*: Al_2O_3).

Table 2
Average size of Co_3O_4 crystallite of catalysts calculated using Scherrer equation

Sample	Crystallite size (nm)
$15Co/Al_2O_3$	18.3
$15Co/0.5Zr/Al_2O_3$	18.2
$15Co/1Zr/Al_2O_3$	19.1
$15Co/5Zr/Al_2O_3$	19.3
$15Co/9Zr/Al_2O_3$	18.4
$15Co/15Zr/Al_2O_3$	20.8

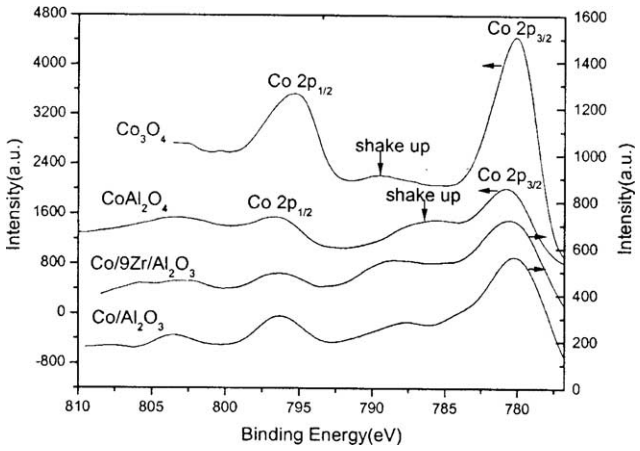

Fig. 2. The Co 2p XP spectra of pure Co_3O_4, $CoAl_2O_4$ and the typical oxidic catalysts.

3.3. X-ray photoelectron spectroscopy (XPS)

The catalysts were investigated by X-ray photoelectron spectroscopy (XPS). The cobalt species on the support is assigned with reference to pure Co_3O_4, $CoAl_2O_4$ (Fig. 2). It can be seen from Fig. 2 that the main peaks (Co $2p_{3/2}$,Co $2p_{1/2}$) of pure $CoAl_2O_4$ exhibit shoulder at the their high binding energy side which can only be ascribed to the shake-up process of Co^{2+} compound in the high spin state, while that of Co_3O_4 is remarkably weak (the Co^{3+}/Co^{2+} ratio is 2:1 in Co_3O_4) because the low-spin Co^{3+} ion does not show shake-up process. It is found that there are strong shake-up satellite observed for all oxidic samples and thereby the main peak (Co $2p_{3/2}$) in these catalysts might be explained by the presence of both $CoAl_2O_4$ and Co_3O_4. In order to determine the intensity of the different cobalt species on the samples, the recorded Co 2p regions were fitted with 80% Gaussian and 20% Lorentzian. The analytical results on Co $2p_{3/2}$ binding energies and the relative intensity of Co compounds are presented in Table 3, while the literature data of various Co-containing compounds are shown in Table 4. As shown in Table 3, the Co $2p_{3/2}$ component at 780.0 eV indicates that the surface cobalt oxide is largely present as Co_3O_4 in these samples. The other component at 782.0 eV can be ascribed to $CoAl_2O_4$. Since all spectra are synthesized under the same fitting method, the XPS intensity ratio of the peaks obtained represents the relative content of the compounds. From Table 3, also, it can be seen that the relative intensity ratio of $CoAl_2O_4/Co_3O_4$ is decreasing with the increase of zirconium content, indicating that the addition of zirconium inhibited the formation of $CoAl_2O_4$. This is consistent with the results of Jongsomjit et al. [17] who studied the Zr-modified catalyst via Raman spectroscopy and concluded that the Zr modification likely prevented the formation of Co "aluminate" on the surface of the catalysts.

Table 4
The XPS data and characteristics of cobalt-containing reference materials [18]

Materials	Co $2p_{3/2}$, BE (eV)	Reliability (eV)
Co	778.1	±0.1
Co_3O_4	780.0	±0.7
$CoAl_2O_4$	781.9	±0.5
$Co(NO_3)_2$	781.9	–

3.4. Temperature programmed reduction (TPR)

The TPR profiles of the catalysts are showed in Fig. 3. Two reduction peaks are exhibited for all samples. The low temperature peak (573–723 K) is typically assigned to the reduction of Co_3O_4 phase ($Co_3O_4 \rightarrow Co^0$) on the surface of the catalysts [14]. Another peak (723–1023 K) of hydrogen consumption is assigned to the reduction of cobalt oxide (Co_3O_4)–alumina interaction species [14,16]. The temperature is not ramped high enough to observe the complete reduction of bulk cobalt aluminate (the stoichiometric $CoAl_2O_4$), which have been shown to occur above 1273 K [6]. Further, no reduction peak of Co–Zr interaction compounds are found.

The peak area (573–723 K) is found to have a progressive increase with the increase of zirconium loading, indicating

Table 3
Co $2p_{3/2}$ binding energy (BE) of different compounds and the relative intensity ratio of $CoAl_2O_4/Co_3O_4$ ($I_{CoAl_2O_4}/I_{Co_3O_4}$) for the prepared oxidic samples

Sample	Co $2p_{3/2}$ BE (eV)				
	Co_3O_4		$CoAl_2O_4$		$I_{CoAl_2O_4}/I_{Co_3O_4}$
	Co $2p_{3/2}$	Intensity (a.u.)	Co $2p_{3/2}$	Intensity (a.u.)	
$15Co/Al_2O_3$	779.81	7718.197	782.03	736.532	0.1962
$15Co/0.5Zr/Al_2O_3$	780.02	2389.48	782.00	459.059	0.1921
$15Co/1Zr/Al_2O_3$	780.03	1844.983	782.19	350.4472	0.1899
$15Co/5Zr/Al_2O_3$	780.24	1878.7	782.0	336.495	0.1791
$15Co/9Zr/Al_2O_3$	780.33	2355.855	782.01	373.376	0.1585
$15Co/15Zr/Al_2O_3$	779.94	2979.751	782.01	360.792	0.1211

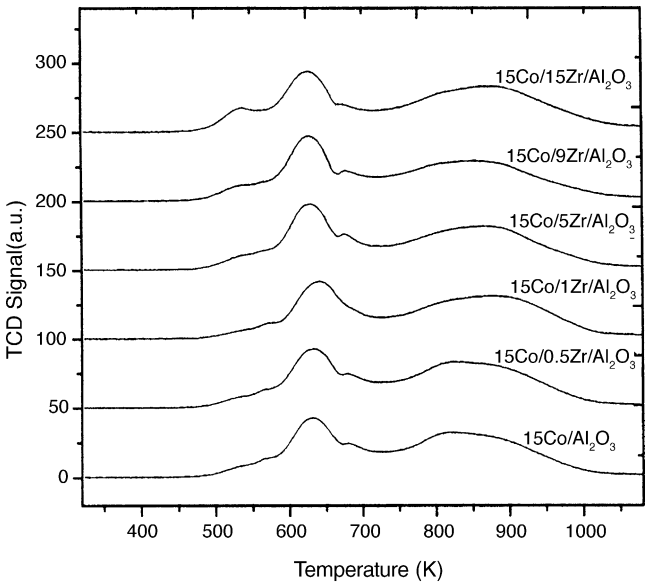

Fig. 3. TPR profiles of samples with different zirconium loading.

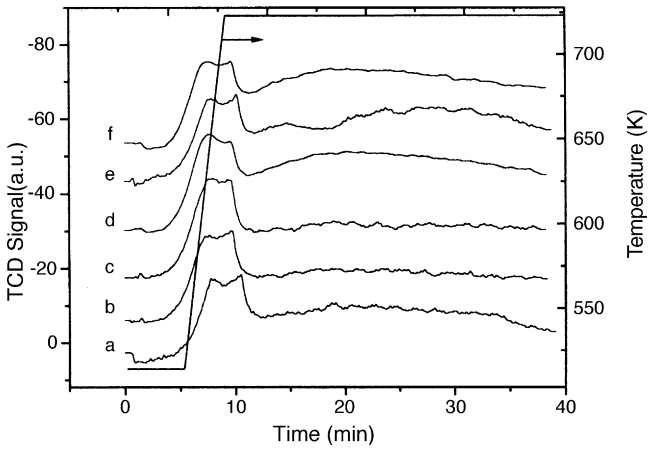

Fig. 4. H_2-TPD profiles of catalysts reduced with different zirconium loading: (a)15Co/Al_2O_3; (b) 15Co/0.5Zr/Al_2O_3; (c) 15Co/1Zr/Al_2O_3; (d) 15Co/5Zr/Al_2O_3; (e) 15Co/9Zr/Al_2O_3; (f) 15Co/15Zr/Al_2O_3.

higher degree of reduction on these catalysts. Meanwhile, it is observed that another reduction peak (723–1023 K) of promoted catalysts is shifted slightly to higher temperature. While with increasing zirconium loading, the hydrogen consumption peak at higher temperature remains essentially constant and the relative peak area of the different temperature region was not significantly changed. Other studies [13,19] have also shown a higher temperature shift for the zirconium promoted catalysts, in agreement with our result. It should be mentioned that the modified samples showed pronounced nitrate peak to the unpromoted Co/Al_2O_3 catalyst by identical prepared process. Rohr et al. [13] have also shown the pronounced peak that was ascribed to the higher affinity to nitrate for the modified catalysts.

3.4.1. *Hydrogen temperature programmed desorption (H_2-TPD) and O_2 titration*

Fig. 4 depicts the H_2-TPD profiles of the catalysts after reduction at 723 K for 12 h. Two hydrogen desorption peaks can be found in these profiles, probably indicating two kinds of hydrogen adsorption sites on the reduced Co catalysts. One peak is located at ca. 623 K and the other is at approximately 723 K. It can be seen that Zr addition has not affected the peak position of hydrogen desorption.

The data for hydrogen temperature programmed desorption and O_2 titration is present in Table 5. The hydrogen chemisorption values are slightly lower at the low zirconium catalysts, while there is an increase in the amount of H_2 chemisorbed with higher zirconium loading and it confirms that more active sites were formed when higher zirconium loading is added. It is also seen from Table 5 that the cobalt dispersion of zirconium-modified catalysts does not increase in comparison with the unpromoted Co catalyst. Similar results have also been found in other study [13]. The obtained results reveal that the metal cobalt cluster size on the catalyst increases due to the addition of zirconium. Here, it should be mentioned that cobalt crystal would be roughened and segregated respectively during Fischer–Tropsch synthesis [20–22]. The dispersion results obtained with the freshly reduced catalyst are not the same as those of the working catalysts. So the dispersion and cluster size data cannot be used to determine the structure sensitivity or structure insensitivity for FTS reaction. Furthermore, the O_2 consumption data showed that the reducibility of the prepared catalysts increase with increasing zirconium

Table 5
H_2-TPD data and O_2 titration data

Sample name	H_2 desorbed (μ mol g^{-1})	d_{uncorr}[a] (%)	D_{uncorr}[b] (nm)	O_2 uptaked (μ mol g^{-1})	d_{corr}[c] (%)	Reducibility (%)	D_{corr}[d] (nm)
15Co/Al_2O_3	88.4	6.94	14.9	898.4	13.2	52.68	7.9
15Co/0.5Zr/Al_2O_3	74.0	5.82	17.7	959.1	10.4	53.24	10.0
15Co/1Zr/Al_2O_3	74.2	5.83	17.5	910.2	10.9	53.37	9.3
15Co/5Zr/Al_2O_3	102.5	8.05	12.8	855.8	16.0	50.18	6.4
15Co/9Zr/Al_2O_3	99.2	7.01	14.7	1005.8	11.9	58.95	8.7
15Co/15Zr/Al_2O_3	100.0	7.73	13.4	1020.4	15.1	59.91	8.0

[a] The uncorrected catalyst dispersion.
[b] The uncorrected metal cluster diameter.
[c] The corrected catalyst dispersion.
[d] The corrected metal cluster diameter.

Table 6
Performances of zirconium-modified Co/Al_2O_3 catalysts in a fixed bed reactor

Catalysts	X_{CO} (%)	Hydrocarbon selectivity (mol%)				
		C_1	C_2	C_3	C_4	C_{5+}
$15Co/Al_2O_3$	32.1	16.2	1.5	2.0	1.39	78.91
$15Co/0.5Zr/Al_2O_3$	32.8	17.7	1.2	1.9	1.35	77.85
$15Co/1Zr/Al_2O_3$	33.0	17.0	1.2	2.0	1.35	78.45
$15Co/5Zr/Al_2O_3$	38.3	15.4	1.2	2.0	1.39	80.01
$15Co/9Zr/Al_2O_3$	39.4	14.6	1.4	2.2	1.43	80.37
$15Co/15Zr/Al_2O_3$	42.6	13.4	1.1	1.6	1.10	82.80

Reaction conditions: 503 K, 1.0 MPa, $CO/H_2 = 1/2$.

content, which has also been revealed by the TPR experiment.

3.5. Fischer–Tropsch synthesis (FTS)

The results of FTS activity and product distribution for the catalysts are listed in Table 6. It can be seen that CO conversion increases with the increase of zirconium loading for all the samples. Similarly, the selectivity to C_{5+} hydrocarbons increases with higher zirconium loading for $Co/Zr/Al_2O_3$ catalysts. Nevertheless, there is not any significant change in C_{5+} selectivity of the hydrocarbon product for the catalysts with low zirconium loading at the reaction conditions. It should be mentioned that the methane selectivity decreases with the increase of zirconium loading.

In this study, the increase in catalyst activity appears to be mainly due to the increase of cobalt active sites and reducibility. Similar to what has been reported by Iglesia [23,24], here, the decrease of the BET surface area of the catalysts and the increase of the surface cobalt active site lead to the increase of the density of Co surface atoms on the support induced by the addition of Zr, enhancing the activity for FTS reaction.

From Fig. 5, a decrease of the ratio of olefin to paraffin is observed with increasing chain length, mainly attributed to the decrease of olefin content. The decrease of olefin content with chain length could be caused by the decrease in the diffusivities of longer chain hydrocarbons. The increase in their residence time in the catalyst pores [25,26], may be caused by α-olefin readsorption [24], or the higher solubility of the higher α-olefin in the liquid phase [27], leading to their increased conversion to paraffin. Furthermore, a significant trend can be observed that the ratio of olefin to paraffin increases with the increase in zirconium loading which has not been observed in previous studies. It concluded that zirconium in cobalt catalysts favored the process of surface restructuring and during self-organization in Fischer–Tropsch synthesis, cobalt sites for secondary olefin reaction increased, whereas sites for chain growth (for monomer formation) decreased by increasing zirconium loading [22]. But this need further experiment to testify.

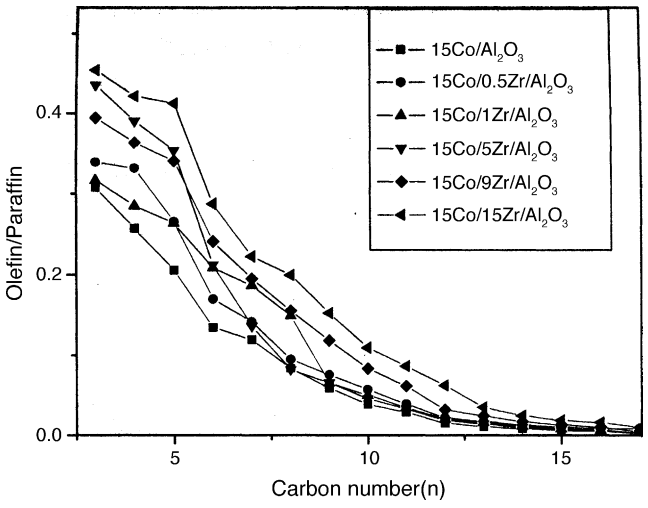

Fig. 5. Influence of zirconium loading on the olefin to paraffin ratio in product of different catalysts.

4. Conclusion

The effect of zirconium at various loading on Co/Al_2O_3 FTS catalyst has been investigated. Cobalt cluster size increased with the addition of zirconium. Increasing zirconium loading effectively inhibited the formation of $CoAl_2O_4$ phase on the catalysts. It gave rise to the increase of Co metal active sites and reducibility, leading to the increase of CO hydrogen activity and C_{5+} selectivity for Fischer–Tropsch synthesis. With increasing zirconium content the methane selectivity was suppressed. The decrease of the ratio of olefin to paraffin in the products with chain growth was attributed to the decrease of the olefin content for all the catalysts. By increasing Zr loading, the ratio of olefin to paraffin in the product tended to increase.

Acknowledgements

This work was supported by the National Natural Science Foundation of China (20373090, 20473114, 20590360), Talented Young Scientist Foundation of Hubei (2003ABB013), Excellent Young Teachers Program of Ministry of Education of China, the State Ethnic Affairs Commission, P.R. China and Returnee Startup Scientific Research Foundation of Ministry of Education of China.

References

[1] J.G. Goodwin Jr, Prep. ACS Div. Petrol. Chem. 36 (1) (1991) 156.
[2] R.J. Madon, E. Iglesia, J. Catal. 139 (1993) 576.
[3] J.L. Zhang, J.G. Chen, J. Ren, Y.H. Sun, Appl. Catal. 243 (2003) 121.
[4] J.L. Li, N.J. Coville, Appl. Catal. 208 (2001) 177.
[5] J.L. Li, G. Jacobs, T. Das, Y.Q. Zhang, B.H. Davis, Appl. Catal. 236 (2002) 67.
[6] J.L. Li, X.D. Zhan, Y.Q. Zhang, G. Jacobs, T. Das, B.H. Davis, Appl. Catal. 228 (2002) 203.
[7] T.K. Das, G. Jacobs, P.M. Patterson, W.A. Conner, J.L. Li, B.H. Davis, Fuel 82 (2003) 805.
[8] G.R. Moradi, M.M. Basir, A. Taeb, A. Kiennemann, Catal. Commun. 4 (2003) 27.
[9] F. Andreas, C. Michael, E. ven Steen, J. Catal. 185 (1999) 120.
[10] H.X. Zhao, J.G. Chen, Y.H. Sun, Chin. J. Catal. 24 (12) (2003), 933.
[11] D.I. Enache, B. Rebours, M. Roy-Auberger, R. Revel, J. Catal. 205 (2002) 346.
[12] S. Ali, B. Chen, J.G. Goodwin Jr., J. Catal. 157 (1) (1995) 35.
[13] F. Rohr, O.A. Lindvaj, A. Holmen, E.A. Blekkan, Catal. Today 58 (2000) 247.
[14] G. Jacobs, T. Das, Y.Q. Zhang, J.L. Li, G. Racoillet, B.H. Davis, Appl. Catal. 233 (2) (2002) 263.
[15] B.D. Cullity, Elements of X-ray Diffraction, 3rd ed., Addison/Wesley, Reading, MA, 1967.
[16] H.F. Xiong, Y.H. Zhang, J.L. Li, Y.Y. Gu, J. Cent. S. Univ. Technol. 11 (4) (2004) 414.
[17] B. Jongsomjit, J. Panpranot, J.G. Goodwin Jr., J. Catal. 215 (2003) 66.
[18] Z. Zsoldos, L. Guczi, J. Phys. Chem. 96 (23) (1992) 9393.
[19] J.L. Zhang, H.X. Zhao, J.G. Chen, J. Ren, Y.H. Sun, Y.N. Xie, T.D. Hu, T. Liu, Chin. J. Catal. 23 (6) (2002) 530.
[20] J.H. Wilson, G.P.M. de Groot, J. Phys. Chem. 99 (1995) 7860.
[21] J.J.C. Geerlings, J.H. Wilson, G.J. Kramer, H.P.C.E. Kuipers, A. Hoek, H.M. Huisman, Appl. Catal. A: Gen. 186 (1999) 27.
[22] H. Schulz, Top. Catal. 26 (2003) 73.
[23] E. Iglesia, Appl. Catal. 161 (1997) 59.
[24] E. Iglesia, S.L. Soled, R.A. Fiato, J. Catal. 137 (1992) 212.
[25] G. Jacobs, K. Chaudhari, D. Sparks, Y.Q. Zhang, B.C. Shi, R. Spicer, T.K. Das, J.L. Li, B.H. Davis, Fuel 82 (2003) 1251.
[26] E. Iglesia, Appl. Catal. 161 (1997) 59.
[27] G.P. Van der Laan, A.A.C.M. Beenackers, Catal. Rev. Sci. Eng. 4 (1999) 255.